31st Annual International Conference of the IEEE EMBS
Minneapolis, Minnesota, USA, September 2-6, 2009

Bioluminescence Tomography with CT/MRI Co-Registration

Klose, A.D. and Beattie, B.J.

***Abstract*—We present a three-dimensional (3D) bioluminescence image reconstruction method with MRI and CT co-registration for small animal molecular imaging. The multi-spectral light intensity distribution of an optical luciferase-luciferin reporter system is measured at the tissue surface of a small animal for the purpose of 3D image reconstruction. The reporter probe distribution inside tissue is calculated with a linear matrix inversion method and a light propagation model based on the simplified spherical harmonics equations. The animal's surface geometry and anatomy is determined from co-registered CT and MR images in order to locate the reconstructed source distribution relative to the animal's anatomy. We present in vivo bioluminescence reconstruction results that demonstrate the performance of our co-registration method.**

INTRODUCTION

BIOLUMINESCENCE imaging is an optical imaging modality for studying disease-associated processes in small animal models. Bioluminescence light is emitted by a luciferase-luciferin reporter system inside tissue and is recorded on the tissue surface by a charged coupled device (CCD) camera. Most experimental studies in bioluminescence imaging are currently performed as monochromatic planar imaging, where light is detected on the tissue surface at a single wavelength. No information about the spatial location of the bioluminescent reporter system can be obtained from these two-dimensional (2D) monochromatic surface images. Moreover, it has been shown that using monochromatic boundary measurements is not sufficient to correctly recover the 3D reporter probe distribution.

In contrast, bioluminescence tomography (BLT) reconstructs the spatial distribution of the optical reporter system by means of 2D surface images and a light propagation model. BLT belongs to the class of emission tomography, which involves the application of computational image reconstruction methods that calculate the unknown physical quantity of interest.[i] The reconstructed physical quantity (e.g. optical source power density in BLT) is subsequently translated into a biologically relevant term of interest (e.g. amount of target cells, concentration of target proteins).

The image reconstruction problem in BLT is most similar to SPECT.[ii] Both imaging modalities reconstruct the density distribution of photon-emitting sources inside tissue from boundary measurements. Low-energy photons at visible wavelengths in BLT are strongly scattered inside tissue, whereas high-energy photons in SPECT encounter only relatively few scattering events. Multiple scattering of photons makes the image reconstruction problem in BLT severely ill-posed. Multi-spectral boundary measurement, however, facilitate the image reconstruction process by increasing the amount of linearly independent measurement data due to the wavelength-dependent extinction coefficient of blood hemoglobin (Fig.1).

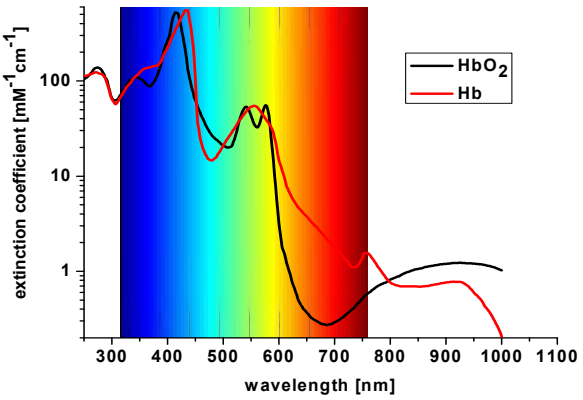

Fig. 1. Extinction coefficient of (oxidized-) hemoglobin inside tissue.

Chaudhari et al.[iii] and Dehghani et al.[iv] have used multiple wavelengths of the bioluminescence spectrum for reconstructing the unknown source distribution with a least-square error approach and were able to obtain 3D reconstructions. Alexandrakis et al.[v] have also found in similar numerical studies that spectrally resolved boundary measurements were necessary to accurately calculate tomographic images of bioluminescent sources.

Besides the difficulties encountered during the image reconstruction process for obtaining the 3D source distribution, BLT does also not reveal the interior tissue structure. Hence, the relative location of the reconstructed source distribution to the animal's anatomy is unknown.

Manuscript received April 23, 2009. This work was supported in part by the National Institutes of Health (NIH) under Grant NCI-U54CA126513-039001.

Alexander D. Klose is with the Department of Radiology at Columbia University, New York, NY 10027 USA (phone: 212-854-5868; fax: 212-854-8725; e-mail: ak2083@columbia.edu).

Bradley J. Beattie is with Memorial Sloan Kettering Cancer Center, New York, NY, 10068, USA. (e-mail: beattieb@mskcc.org).

Therefore, light propagation models in BLT either assume a uniform distribution of optical properties or employ approximate tissue maps based on poorly constrained warping of segmented numerical mouse phantoms. Investigators have attempted to incorporate such information based on a numerical mouse model (Digi-Mouse) but thus far these efforts have involved rough, generic approximations of the organ placements, not the imaged animal's actual measured tissue distributions.[vi] These inaccurate tissue models could lead to false light predictions on the skin surface and thus incorrect image reconstructions.

Co-registration to anatomical image sets (e.g. MR and CT images) would allow for the incorporation of information regarding the actual distribution of the various tissue types within the mouse (e.g. liver, kidneys, bones) into the BLT reconstruction and would also provide an anatomical reference for the reconstructed probe distribution.

I. BIOLUMINESCENCE IMAGE RECONSTRUCTION

A. Light Propagation Model

Current studies in BLT assume the validity of the diffusion approximation to the equation of radiative transfer (ERT). There is ample evidence, however, that this low-order approximation to the ERT is only valid when applied to wavelengths in the region larger than 600nm where attenuation in biological tissues is much less than scatter. The large absorption coefficients of tissue hemoglobin at wavelengths smaller than 600 nm (Fig. 1) make the diffusion model less accurate.[vii] The diffusion model is also less accurate when imaging small tissue geometries (optical thickness less than 20 transport mean free paths) where boundary effects become significant.

Our light propagation model, F, is based on the simplified spherical harmonics (SP_N) equations that are a high order approximation to the ERT and, hence, overcomes the limits of the diffusion equation when large light absorption and small geometries are present. We numerically solve the SP_3 equations (N=3) with a finite-difference method on a Cartesian grid. Thus, we can deal with non-uniform optical properties of tissue, defined on grid points of the computational domain, and with curved geometries, approximated by grid points close to the physical tissue boundary. Numerically solving the SP_3 equations does only require 2.5 times the computational effort than solving the diffusion equation alone. A solution of the SP_3 equations yields the partial current of light, J^+, on the tissue surface for given light sources, Q, and optical tissue properties, μ. The SP_3 equations are given by two coupled diffusion equations:

$$-\nabla\cdot\frac{1}{3\mu_{a1}}\nabla\varphi_1+\mu_a\varphi_1=Q+\frac{2}{3}\mu_a\varphi_2 \qquad (1)$$

$$-\nabla\cdot\frac{1}{7\mu_{a3}}\nabla\varphi_2+\left(\frac{4}{9}\mu_a+\frac{5}{9}\mu_{a2}\right)\varphi_2=-\frac{2}{3}Q+\frac{2}{3}\mu_a\varphi_1 \qquad (2)$$

The moments of the absorption coefficients are given by $\mu_{an} = \mu_a + \mu_s - \mu_s g^n$, with g being the anisotropy factor, μ_a and μ_s being the absorption and scattering coefficients. Q depicts the interior bioluminescent source. Both coupled equations (1) and (2) are solved on a 3D *Cartesian* grid with a finite-difference method. A solution can be obtained in less than approximately 2 seconds for 10,000 grid points. More details can be found in Klose and Larsen.[viii]

B. Linear Matrix Inversion

We reconstruct the unknown bioluminescent sources Q from the given partial current J^+ and optical parameters μ. The relation $Q=F^{-1}(\mu,J^+)$ is indirectly solved by casting Q and J^+ into vectors and $F(\mu)$ into a matrix.[ix] A set of algebraic equations, $\boldsymbol{J}=\boldsymbol{FQ}$, is solved for the unknown vector $\boldsymbol{Q}$ with an algebraic reconstruction technique (ART). The matrix $\boldsymbol{F}$ is computed by solving the SP_3 equations for a set of unit sources defined at all Cartesian grid points and a uniform tissue model described by the average parameters μ_s and μ_a. The optical parameters were reconstructed for a uniform medium given a known source location and multispectral boundary data. The solution, $\boldsymbol{Q}$, is displayed in a set of images.

II. IMAGE CO-REGISTRATION

We have developed a co-registration procedure to relate the coordinate spaces of an IVIS 200 bioluminescence imager (Caliper Sciences) with those of our microCT (Siemens) and small animal MRI (Bruker) scanners. This, coupled with a means of maintaining the mouse in a rigid pose while affixed to a bed that can be moved between scanners, allows for precise co-registration of the image information from each modality. The details of these procedures will be given below.[x]

The overall objective of our procedures is to base the registrations on a calibrated positioning of the animal within each scanner's field of view. Between and during the imaging sessions, the animal is held in a rigid pose, at a fixed position relative to the animal bed. This is accomplished by wrapping the animal with a thin 0.01 mm polyethylene wrap while it is positioned atop a custom designed bed with a nose cone for the administration of oxygen and gaseous anesthesia. The wrap applies a light pressure over the entire body of the animal, gently and efficiently restricting its movement. Registration then amounts to establishing a frame of reference relative to the bed for each scanner and calculating the rigid or projective transforms that map between them.

The Siemens microCT scanner has a motorized bed positioning mechanism with optically encoded position readout calibrated to a precision of 0.01 mm and a repositioning accuracy of better than 0.1 mm. A custom adapter is used to attach the animal bed to this bed positioning mechanism in a reproducible manner. It can then be removed for placement on the other scanners using specialized bed mounts designed for each. The coordinate system defined by the microCT's bed positioning mechanism was used as the reference frame to which both the Bruker and IVIS images are mapped.

Positioning of an animal within the field of view of the Bruker does not easily lend itself to such reproducibility because its field of view is located deep within its bore and thus is remote from any potential spatial reference. References within the bore are generally blocked by the gradient and readout coils. Therefore, we established a set of markers within the bed that are visible both on MR and CT. Using landmarks derived from these markers we can place the MR image set into the microCT's frame of reference. Alternatively, retrospective mutual information based volume registration methods work well when registering these two structural image datasets to one another. For the IVIS, we constructed a bed mount that includes a platform referencing two of the inside edges of the IVIS' light-tight box. Thus, the bed mount and the attached bed can be consistently placed within the IVIS, thereby allowing precisely reproducible positioning of the animal relative to the camera for any given camera to subject distance. The bed and its mounting system were designed such that the bed can be pivoted about its long axis (inferior to superior axis of the mouse) in precisely calibrated 15° increments, allowing views of the animal from different vantage points

A. *Bioluminescence imaging camera model*

The camera model we used was that of a basic pinhole camera as described by Hartley and Zisserman.[xi] In this model, points in 3D space represented in homogenous coordinates $(X,Y,Z,T)^T$ are mapped onto the 2D image plane by the 3×4 projective transformation matrix which is parameterized as follows:

$$\begin{bmatrix} f & 0 & p_u \\ 0 & f & p_v \\ 0 & 0 & 1 \end{bmatrix} \bullet [R_{xyz}] \bullet \begin{bmatrix} 1 & 0 & 0 & c_x \\ 0 & 1 & 0 & c_y \\ 0 & 0 & 1 & c_z \end{bmatrix} \bullet \begin{bmatrix} \cos\beta & 0 & -\sin\beta & 0 \\ 0 & 1 & 0 & 0 \\ \sin\beta & 0 & \cos\beta & 0 \\ 0 & 0 & 0 & 1 \end{bmatrix} \bullet [Q_{xyz}] \bullet \begin{bmatrix} 1 & 0 & 0 & t_x \\ 0 & 1 & 0 & 0 \\ 0 & 0 & 1 & t_z \\ 0 & 0 & 0 & 1 \end{bmatrix}$$

Here, R_{xyz} and Q_{xyz} are rotation matrices having three parameters each. Point (p_u,p_v) is the center of the acquired image, (c_x,c_y,c_z) is the camera center, and β describes the rotation of the bed about its axis. Vector $(t_x,0,t_z)$ defines the translation which when combined with Q_{xyz} moves the bed from its position in the CT coordinate system onto the axis of the bed-mount in the bioluminescence imaging coordinate system. Parameters p_u, p_v and β are fixed, while the 12 remaining parameter values are determined in a calibration procedure.

The radial distortion of the bioluminescence camera lens is modeled as a Taylor expansion (shown below with three terms) of an arbitrary function of r, the distance from (p_u,p_v). Parameters a, b and c are determined in a separate calibration procedure using a photographic image of a rectilinear grid.

$$\begin{aligned} r^2 &= (u - p_u)^2 + (v - p_v)^2 \\ \hat{u} &= (u - p_u) \cdot (1 + ar + br^2 + cr^3) + p_u \\ \hat{v} &= (v - p_v) \cdot (1 + ar + br^2 + cr^3) + p_v \end{aligned} \tag{4}$$

B. *Camera model calibration*

Grids cut into plastic block are visible on both CT and in photographs taken by the IVIS camera system. Homologous points within the two datasets are manually identified. Photographs within the bioluminescence system are taken at multiple bed angles. The CT derived points are transformed by the camera model and the distance between pairs of homologous points is minimized in an iterative procedure.

C. *Registration results*

The camera model allows information to be passed back and forth between the 2D and 3D image domains. For example it can be used to render virtual 2D images from the information in the 3D datasets that are registered to the 2D bioluminescence images taken by the IVIS. Figure 2 shows a series of MR slices (in gray-scale) which going from left to right are taken at progressively further distances from the modeled camera system. All are registered to the bioluminescence image which is superimposed in a pseudo-color color-scale along with a transparent skin surface determined from a registered CT dataset. Beneath the bioluminescence image hot-spots over the shoulder and midsection, are two tumors that are the source of the bioluminescence.

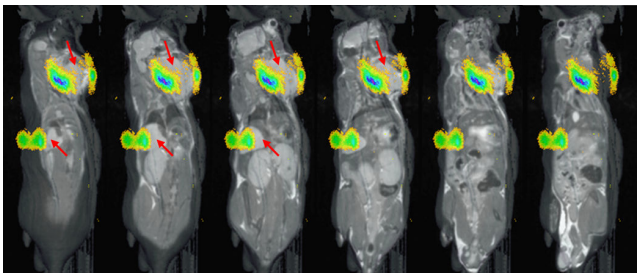

Fig. 2: Bioluminescence light distribution on animal surface for different vantage points. Light originates from two tumors.

The accuracy of the registration can also be appreciated by examination of Figure 3. We were using a surrogate for the bioluminescent source whose position could be precisely determined within the CT image sets and whose intensity was precisely known. Gaseous tritium light source (GTLS) beads emit light at a virtually constant intensity powered by tritium decay. The beads used here are 0.9 mm x 2.3 mm glass cylinders. They come in a variety of colors. For the

studies shown here, a yellow bead was inserted into a catheter which in turn was placed into the animal's rectum via a catheter. The GTLS bead emits light over a range of 100 nm with a peak at 531nm mimicking the spectrum of a luciferase-luciferin reporter system.

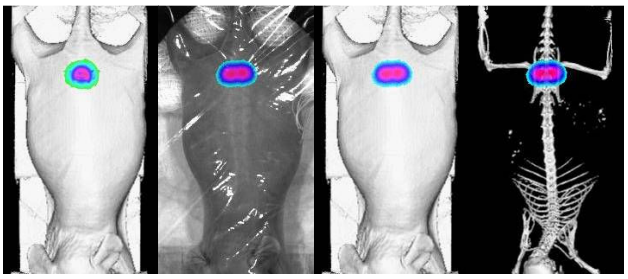

Fig. 3. From left to right: Luminescence light propagation simulation based on the SP_3 equations, reflectance image with superimposed measured luminescence image, surface rendered CT image with superimposed measured luminescence light image, and CT image of skeleton with superimposed measured luminescence image.

The leftmost image in Figure 3 is a light propagation simulation. Next to it is the standard reflectance light image of the mouse onto which has been superimposed the bioluminescence image taken moments later with the same camera system. The third image from the left contains the same bioluminescence data but this time superimposed upon a surface rendered image of the mouse skin derived from a registered CT dataset. Likewise, in the right-most image it is the skeleton of the mouse that is surface rendered. The animal was placed inside the IVIS system.

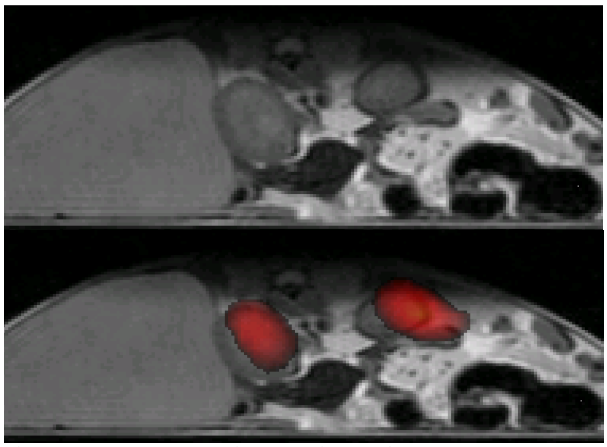

Fig. 4. BLT reconstruction superimposed onto MRI. Top: MRI. Bottom: fused BLT reconstruction with MRI. Bioluminescent reporter probe signal is seen in both kidneys.

III. In vivo results

A transgenic animal had been engineered such that its kidneys would constitutively express click-beetle red (CBR) luciferase. A set of multi-spectral bioluminescence (580, 600, 620, 640, 660 nm) images and an MR scan of the mouse were acquired and registered to one another, as shown in Figure 4. The acquisition time for taking all bioluminescence images was about 20 minutes. BLT reconstructions of this dataset were conducted using our SP_3 model. Together these images demonstrate the importance of including information regarding the actual co-registered mouse anatomy relative to the reconstructed reporter probe distribution.

Acknowledgment

This work was supported in part by grant (NCI-U54CA126513-039001) from the National Institutes of Health.

[i] D. Gourion, D. Noll, "The inverse problem of emission tomography," Inverse Problems 18, 1435-1460 (2002).

[ii] P.P. Bruyant, "Analytic and iterative reconstruction algorithms in SPECT," The Journal of Nuclear Medicine 43(10), 1343-1358 (2002).

[iii] A.J. Chaudhari, F. Darvas, J.R. Bading, R.A. Moats, P.S. Conti, D.J. Smith, S.R. Cherry, R.M. Leahy, "Hyperspectral and multispectral bioluminescence optical tomography for small animal imaging," Physics in Medicine and Biology 50, 5421-5441 (2005).

[iv] H. Dehghani, S.C. Davis, S. Jiang, B.W. Pogue, K.D. Paulsen, "Spectrally resolved bioluminescence optical tomography ," Optics Letters 31(3), 365 (2006).

[v] G. Alexandrakis, F.R. Rannou, A.F. Chatziioannou, "Tomographic bioluminescence imaging by use of a combined optical-PET (OPET) system: a computer simulation feasibility study," Physic in Medicine and Biology 50, 4225-4241 (2005).

[vi] G. Wang, W. Cong, K. Durairaj, X Qian, H. Shen, P. Sinn, et al. "In vivo mouse studies with bioluminescence tomography," Optics Express 14(17), 7801-7809 (2006).

[vii] A.H. Hielscher, R.E. Alcouffe, R.L. Barbour, "Comparison of finite-difference transport and diffusion calculations for photon migration in homogeneous and heterogeneous tissue," Physics in Medicine and Biology 43, 1285-1302 (1998).

[viii] A.D. Klose and E.W. Larsen, "Light transport in biological tissue based on the simplified spherical harmonics equations," Journal of Computational Physics 220, 441-470 (2006).

[ix] A.D. Klose, "Radiative transfer of luminescence light in biological tissue," in: Light Scattering Reviews, Vol. 4, A.A. Kokhanovsky (Ed.), 293-345, Springer, Berlin, 2009.

[x] B.J. Beattie, A.D. Klose, C.H. Le, V.A. Longo, K. Dobrenkov, J. Vider, J.A. Koutcher, R.G. Blasberg, "Registration of planar bioluminescence to magnetic resonance and x-ray computed tomography images as a platform for the development of bioluminescence tomography reconstruction algorithms," Journal of Biomedical Optics 14(2), 024045 (2009).

[xi] R. Hartley, A. Zisserman, "Multiple view geometry in computer vision," 2nd Ed., Cambridge University Press, 2004.